Bioorganic Chemistry 115 (2021) 105185

Contents lists available at ScienceDirect

Bioorganic Chemistry

journal homepage: www.elsevier.com/locate/bioorg

Selective inhibition of *Helicobacter pylori* methionine aminopeptidase by azaindole hydroxamic acid derivatives: Design, synthesis, *in vitro* biochemical and structural studies

Sandeepchowdary Bala [a,b,1], Kalisha vali Yellamanda [c,1], Anilkumar Kadari [c], Venkata.S. U. Ravinuthala [a], Bhavita Kattula [a,b], Om V. Singh [c], Rambabu Gundla [c,*], Anthony Addlagatta [a,b,*]

[a] Division of Applied Biology, CSIR-Indian Institute of Chemical Technology, Hyderabad 500 007, Telangana, India
[b] Academy of Scientific and Innovative Research (AcSIR), Ghaziabad, Uttar Pradesh 201 002, India
[c] Department of Chemistry, School of Science, GITAM Deemed to be University, Hyderabad 502 102, Telangana, India

ARTICLE INFO

Keywords:
Methionine aminopeptidase
Selective inhibition
Azaindole
Hydroxamic acid
Helicobacter pylori

ABSTRACT

Methionine aminopeptidases (MetAPs) are an important class of enzymes that work co-translationally for the removal of initiator methionine. Chemical inhibition or gene knockdown is lethal to the microbes suggesting that they can be used as antibiotic targets. However, sequence and structural similarity between the microbial and host MetAPs has been a challenge in the identification of selective inhibitors. In this study, we have analyzed several thousands of MetAP sequences and established a pattern of variation in the S1 pocket of the enzyme. Based on this knowledge, we have designed a library of 17 azaindole based hydroxamic acid derivatives which selectively inhibited the MetAP from *H. pylori* compared to the human counterpart. Structural studies provided the molecular basis for the selectivity.

1. Introduction

Ribosome assisted protein synthesis in almost all living cells begins with the amino acid methionine in eukaryotes while it is formyl methionine in prokaryotes [1,2]. Methionine aminopeptidase (MetAP) class of enzymes cleave the initiator methionine in 60–70% of proteins in all living cells [3,4]. In prokaryotes, the peptide deformylase (PDF) removes the *N*-terminal formyl group before the methionine hydrolysis [5]. Both these hydrolytic processes on the amino-terminus at the ribosome exit tunnel are essential for the survival of all living cells [6]. Most prokaryotes contain a single gene of *map* while eukaryotes have redundant genes. Chemical inhibition or gene knockout in *E. coli* and other microbes was detrimental [7,8]. Eukaryotic cytosolic MetAP proteins are classified as Type 1b and Type 2 while the mitochondrial MetAP is classified as Type 1d. Deletion of a single map gene in eukaryotes results in slow growth phenotypic cells but detrimental when both were deleted [8]. Natural product fumagillin family compounds that include ovalicin inhibit Type 2 MetAP by a million-fold better than Type 1 enzyme, suggesting that there are differences between the two active sites [9,10]. All prokaryotes contain only Type 1 MetAPs. Depending upon N-terminal extensions or insertions within the Type 1 *map* genes, these have been sub-classified as Type 1a, 1b, 1c, 1d, and 1n (**Fig. S1**) [11]. All MetAPs are metalloenzymes and the active site accepts at least two metal ions from first row transition elements. Because of their criticality, MetAPs are identified as good drug targets in antimicrobial and anticancer therapies.

Since prokaryotic MetAPs are good antibacterial targets, several studies have been reported to identify inhibitors [12,13–15]. However, the biggest challenge is in selective inhibition of microbial enzymes because of the similarity of their active site with human enzyme [12,13]. For more than a decade, others and we have studied active sites of a large number of MetAPs from microbes, specifically from point of view of inhibitor selectivity [12,13,16–24]. Based on our earlier studies, we have identified that the S1 pocket could be separated into two parts: a

Abbreviations: AMC, 7-Amido-4-methylcoumarin; HATU, (1-[Bis(dimethylamino)methylene]-1H-1,2,3-triazolo[4,5-b]pyridinium 3-oxide hexafluorophosphate.

* Corresponding authors.
E-mail addresses: rgundla@gmail.com (R. Gundla), anthony@csiriict.in (A. Addlagatta).

[1] Authors equally contributed to work

https://doi.org/10.1016/j.bioorg.2021.105185
Received 1 March 2021; Received in revised form 4 June 2021; Accepted 14 July 2021
Available online 21 July 2021

conserved and a variable lobes. Based on these fine differences, we have identified selective inhibitors against MetAP from pathogenic microbes [12,13].

Almost half of the world's population is infected with *H. pylori* [25]. It is a spiral shaped gram-negative bacterium that grows in the digestive tract. *H. pylori* invade the stomach lining causing ulcer formation which in turn has a high risk of stomach cancer. Eradication of *H. pylori* has been difficult due to its drug resistance towards antibiotics (amoxicillin, clarithromycin, and other drugs metronidazole) [26]. Triple therapy such as levofloxacin or rifabutin in combination with amoxicillin and esomeprazole has been used to overcome the drug resistance curing nearly 90% of the cases [26]. There is a necessity for new drugs that can selectively and effectively target the *H. pylori* enzymes. Based on our earlier understanding, we identified *H. pylori* MetAP1a (*Hp*MetAP1a) as a starting point to discover specific inhibitors against this organism. We have designed and synthesized a library of 17 compounds that contain hydroxamic acid moiety as a metal binding scaffold. Using biochemical and structural biology tools we have determined molecular insights into selective inhibition of enzyme from *H. pylori* compared to the human counterpart.

2. Materials and methods

2.1. Materials

Phusion high fidelity DNA polymerase was obtained from NEB (USA) while Taq DNA polymerase was obtained from LAADH Biotech Pvt. Ltd, Hyderabad, India. All oligonucleotides were procured from BioArtis Life Sciences Pvt. Ltd, Hyderabad. All buffers, fine chemicals, solvents, and substrates used for synthesis and enzyme assays were obtained from Sigma-Aldrich (USA), SRL (India), GenPro Biotech (India), Alfa Aesar (India), and TCI (India).

2.2. Cloning

map gene (UniProt ID: P56102) was amplified from the genomic DNA of *H. pylori* (ATCC 26695) using polymerase chain reaction and cloned into the pET15b vector using the *Nde*I and *BamH*I restriction sites. The Δ91 human MetAP1b (*Hs*MetAP1b) which is devoid of the *N*-terminal zinc fingers is used in the present study. Details about its characterization and biochemistry are published elsewhere [12,27]. A list of oligos used in this study is given in the Supplementary Information (**Table S1**).

2.3. Protein expression and purification

Purification of *Hs*MetAP1b was performed as described previously (**Fig. S2**) [12]. A similar method was followed for the *Hp*MetAP1a. Briefly, the pET15b plasmid was transformed into BL21 (DE3) *E. coli* strain for protein expression. A single colony was inoculated in LB broth having 50 μM of ampicillin. The overnight culture was added to four liters of LB media and incubated at 37 °C by shaking at 250 rpm. Protein expression was induced by the addition of IPTG to a final concentration of 1.0 mM and incubated at 25 °C by shaking at 150 rpm for 16 h. The bacterial cell pellet was collected by centrifugation of the culture at 6,000*g* for 20 min at 4 °C. The cell pellet was resuspended in 50 mL of buffer A(50 mM HEPES buffer pH 8.0 150 mM NaCl, 0.1% Triton X-100, 10% glycerol, and 10 mM imidazole), in the presence of protease cocktail inhibitor (5 mg), 50 mg of lysozyme, 10 mg of DNase and 2.5 mM of $MgCl_2$. After lysozyme treatment, the cell suspension was subjected to sonication (sonicator with model number PKS-250F (PCI Analytics Pvt. Ltd.)) with a frequency of 20 kHz and power 250 W and with a probe diameter of ¼ inch (70% amplitude at 4 °C, 10 min (2 s on and 4 s off)) to achieve complete lysis. Cell debris was removed by centrifugation at 35,000*g* for 40 min. The lysate was passed through a nickel NTA affinity column pre-equilibrated with buffer A. After passaging the lysate, the column was washed with buffer A until the absorption at OD_{280} reached zero. Continued the column wash with buffer B (50 mM HEPES buffer pH 8.0, 150 mM NaCl and 10 mM imidazole) until the absorption at OD_{280} reached zero. Pure protein was eluted by gradient elution of imidazole (10 mM–200 mM) in buffer B. Pooled fractions were dialyzed into storage buffer (25 mM HEPES pH 8.0 and 150 mM NaCl), concentrated to 10 mg/ml, and stored at −80 °C until further use.

2.4. Effect of different metal ions on enzyme activity

*Hs*MetAP1b was shown to be active in the presence of Co^{2+} [12,27]. Metal selectivity was tested for *Hp*MetAP1a (5 μM of the enzyme) using various concentrations (1–1000 μM) of divalent metal ions (Ni^{2+}, Co^{2+}, Mn^{2+}, and Zn^{2+}) in 25 mM HEPES pH 8.0 and 150 mM NaCl and incubated for 20 min at 37 °C. After incubation for 30 min, 50 μM of methionine 7-amino-4-methyl coumarin (Met-AMC) was added to the reaction and the release of free AMC was monitored continuously using a microtiter plate reader (TECAN, Austria) with excitation and emission wavelengths of 380 nm and 460 nm, respectively.

2.5. Determining the optimum pH

The effect of pH on the activity of *Hp*MetAP1a was determined using acetate buffer (pH 5.0, 5.5), sodium phosphate buffer (pH 6.0 and 6.5), HEPES (pH 7.0, 7.5 and 8.0), Tris (pH 8.5) and sodium carbonate (pH 9.0) at 25 mM concentration with 1 μM of the enzyme, two equivalents of $NiCl_2$, and 50 μM of methionine 7-amino-4-methyl coumarin (Met-AMC).

2.6. Determining the substrate specificity

AMC derivatives of various amino acids) (Asp, Asn, Ala, Glu, Gln, Arg, His, Ile, Leu, Lys, Met, Ser, Phe, and Thr) were used to test the activity of the *Hp*MetAP1a. All substrates used for this study have free amino terminus.). Reactions were carried out with a final volume of 100 μl having 25 mM HEPES (pH 8.0), 150 mM NaCl, 5 μM of *Hp*MetAP1a, 200 μM of substrate concentration, and two equivalents of $NiCl_2$, in a 96-well black flat-bottom microtiter plate (Corning Inc., USA) at 37 °C. Kinetic studies were carried out using different concentrations of substrates and the data were analyzed using SigmaPlot 13.0.

2.7. Enzyme kinetics

The K_M and k_{cat} of *Hp*MetAP1a towards Met-AMC in the presence of $NiCl_2$ were determined (**Table S2**). At a fixed concentration of 5 μM of *Hp*MetAP1a, the substrate concentration was varied between 25 μM and 1200 μM and the reaction was performed at 37 °C in triplicates. K_M and V_{max} were determined from slopes of various concentrations of the substrate by applying a non-linear curve fit analysis. The turnover number and k_{cat} values were determined manually by applying the formula $k_{cat} = V_{max}/[E]$, where V_{max} is the maximum velocity and [E] is the total enzyme concentration. Data were fitted against the Michaelis-Menten equation: $v = V_{max} \times [S]/(K_M + [S])$, using SigmaPlot.

2.8. Inhibitor studies

10 mM stocks of compounds were prepared in dimethyl sulfoxide (DMSO) solution. Initially, all compounds were tested for inhibition of the enzyme at 10 μM against MetAP enzymes from *H. pylori*, *E. coli*, *V. coralliilyticus*, *S. pneumoniae,* and human MetAP1b (**Table S6**). *K*i values for the compounds within the range of tight binding inhibition were determined (using the Morrison method) [28] by fitting the data using non-linear regression in the formula listed below.

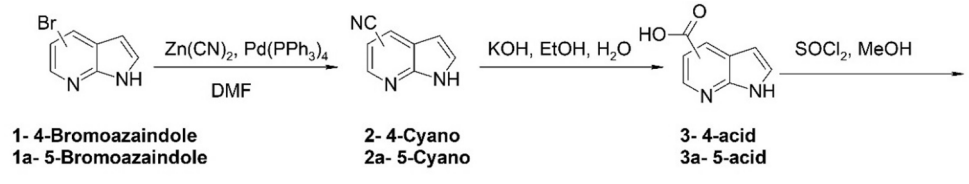

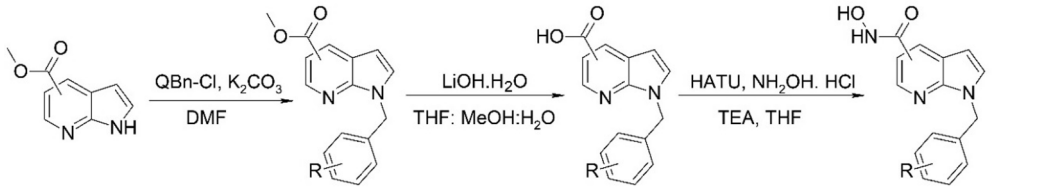

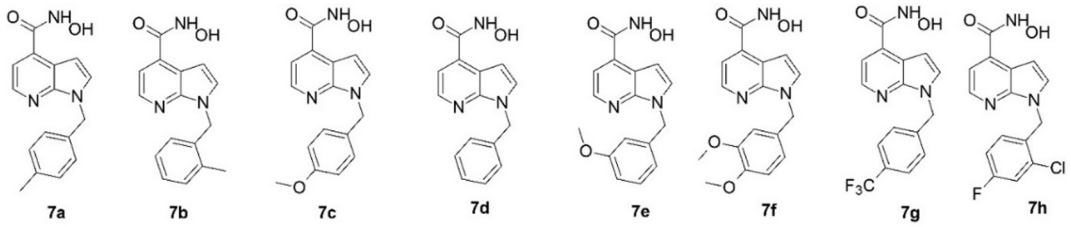

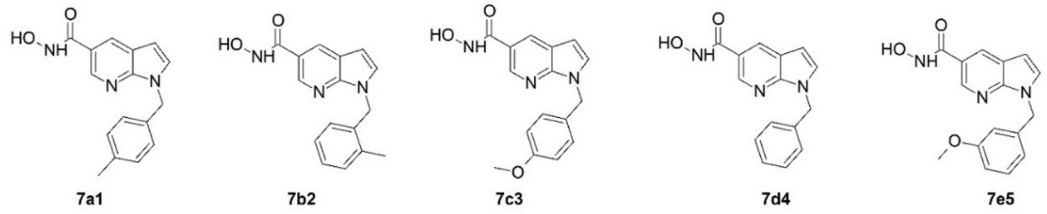

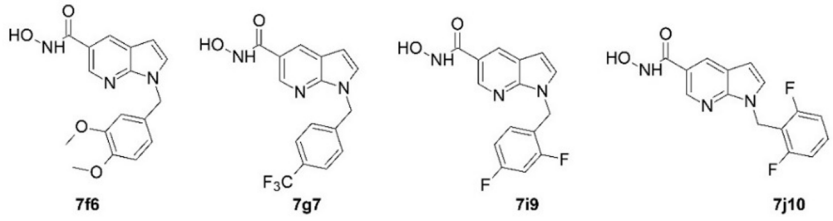

$$\frac{v_i}{v_0} = 1 - \frac{\left([E] + [I] + \left(K_i\left(1 + \frac{[S]}{K_M}\right)\right)\right) - \sqrt{\left([E] + [I] + \left(K_i\left(1 + \frac{[S]}{K_M}\right)\right)\right)^2 - 4[E][I]}}{2[E]}$$

2.9. Crystallization and X-ray data collection

Crystallization of *Hp*MetAP1a was set up with 12 different crystallization screens (Hampton research and Molecular Dimensions), which corresponds to about 1,200 reagents. No condition yielded diffraction quality crystals. Crystallization of *Hs*MetAP1b was set up using the following method: 10 mg/ml protein in storage buffer was mixed in 1:1 ratio with well solution (0.1 M BISTRIS pH 6.2, 19% PEG 3350, and 5% glycerol) and incubated at 25 °C. Rod-like crystals appeared in 24–48 h. Cryoprotectant solution was prepared with 25% glycerol in well solution. Crystals were soaked with cobalt and compound **7d** or compound **7e5**. Single Crystal was frozen in the stream of liquid nitrogen and shipped to Elettra Synchrotron, Trieste, Italy. X-ray diffraction data were collected on the XRD2 beamline. Diffraction data were processed and scaled using XDS [29]. Since all structures were homologous to the wild-type *Hs*MetAP1b structure, they were directly refined using the 2B3H PDB [30] coordinates using the REFMAC5 [31] in the CCP4 [32] crystallographic suite after removing all water molecules. Structure

Table 1
Showing active site residue variations within Type 1 methionine aminopeptidase.

S. No	Left lobe	Right lobe
1	Site-1 (P-192): P(40.76), F(19.23), Y(16.38), N(5), T (4.61), L(3.53), Q(3.46), S(2.76), C(2.23), E(1.53), A (0.153), G(0.153), R(0.07)	F(73.5),Y(26.5)
2	Site-2 (Y-195): Y(72.46), P(5.53), T(5.153), C(3.61), G(3.07), N(2.07), F(1.92), V(1.07), S(0.53), L(0.61), D(0.69), E(0.384), Q(0.15), A(0.15), I(0.15), H (0.076), M(0.07)	C(97),N(2.53), L (0.30),T(0.15)
3	Site-3 (F-309): F(59.30), M(17), L(12.84), Y(5.38), I (2.30), V(1.30), P(0.07)	W(100)

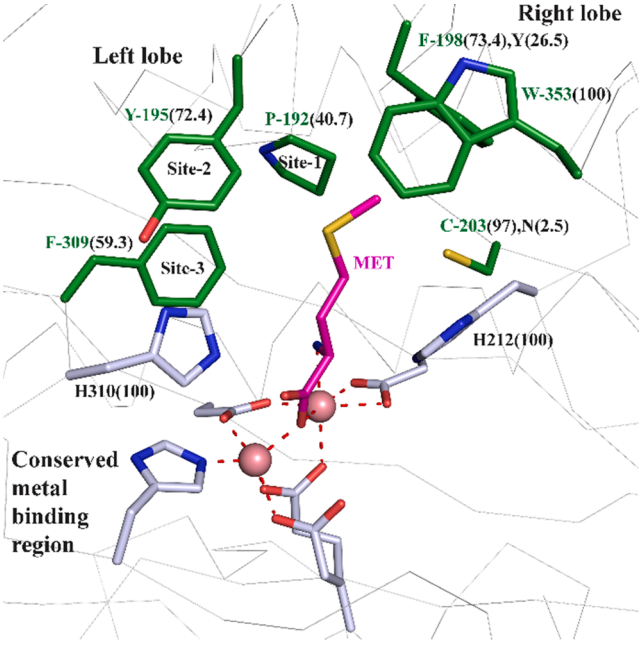

Fig. 1. Active site residue variations among Type 1 methionine aminopeptidases S1 pocket residues are shown in sticks (green) (PDB ID: 4U6J) are shown. Metal-binding residues and gatekeeper residues are shown in grey. (For interpretation of the references to colour in this figure legend, the reader is referred to the web version of this article.)

modeling against observed structure factors was performed in COOT [33]. All graphics generated for this manuscript were prepared using Pymol [34].

2.10. Homology modeling

SWISS-MODEL [35] is used to generate 3D homology models of proteins which is a web-based bioinformatics tool. The homology model of the *Hp*MetAP1a was built using *Hs*MetAP1b (PDB ID: 4U6J) as a template (32.7% sequence identity) (**Fig. S3**). The model was validated using the RAMPAGE [36] (**Fig. S4**) for the assessment of the Ramachandran plot.

2.11. Docking of azaindole hydroxamic acid derivatives on human Type 2 MetAP

Docking studies were carried out on the crystal structure of MetAP2 (PDB ID: 2ADU) (Fig. 6a and 6b) [37]. Protein was prepared for docking by removing the ligand and water molecules. The coordinates for ligand molecules were generated using the PRODRG server [38]. The input files for AutoDock Vina [39] were generated after adding polar hydrogens

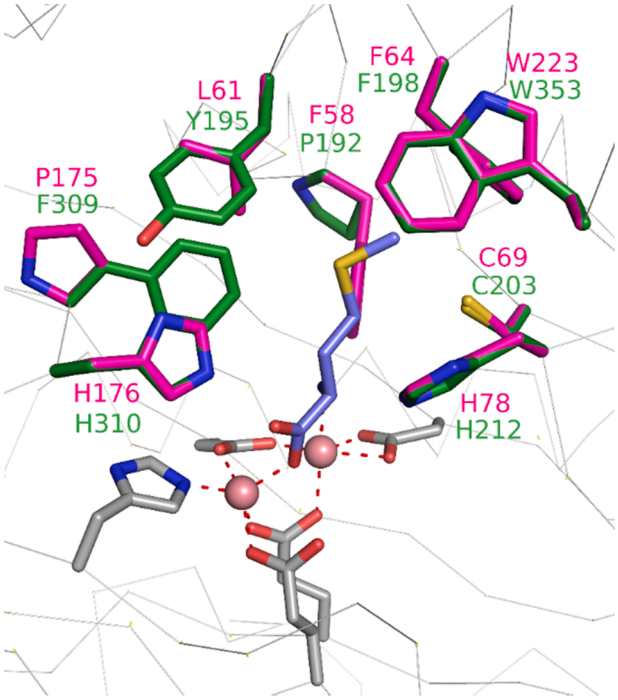

Fig. 2. Structural alignment showing S1 pocket residues of *Hs*MetAP1b in sticks (green) in complex with methionine (violet) (PDBID: 4U6J) and *Hp*MetAP1a (pink) homology model. (For interpretation of the references to colour in this figure legend, the reader is referred to the web version of this article.)

and Gasteiger charges, using AutoDock Tools [40] of the MGLTools package. A cube with a side of 14 Å was used for generating 20 docking poses. Visualized the docking poses and generated representative figures using open-source PyMOL [34].

2.12. Chemistry

The chemistry used for the formation of azaindole esters **5a-5h** and **5a1-5j10**, azaindole acids 6**a-6h** and **6a1-6j10**, and final products **7a-7h and 7a1-7j10** are depicted in Schemes 1 and 2. Bromo azaindole was converted to the corresponding cyano with zinc cyanide in the presence of catalytic amounts of $Pd(PPh_3)_4$ provided nitrile **2** and **2a**, which was converted to acid **3** and **3a** followed by esterification to provide ester **4** and **4a**. Azaindole esters were alkylated using benzyl halides and potassium carbonate to provide esters **5a-5h** and **5a1-5j10**. Saponification of esters with $LiOH{\cdot}H_2O$ provided acids 6**a-6h** and **6a1-6j10**. Hydroxamic acids **7a-7h** and **7a1-7j10** were prepared by treatment of hydroxylamine hydrochloride by using HATU and triethylamine to get corresponding *N*-alkylated hydroxamic acids.

Scheme for the synthesis of azaindole hydroxamic acid derivatives:

Target molecules:

Nuclear magnetic resonance spectra (^1H NMR: 400 MHz and ^{13}C NMR: 100 MHz) were recorded in $CDCl_3$ and DMSO-d_6 using an Avance III 400 MHz spectrometer (Bruker). Chemical shifts are reported in parts per million (ppm) and the coupling constants (J) are expressed in Hertz (Hz). Splitting patterns are designated as follows: s, singlet; d, doublet; t, triplet; q, quadruplet; m, multiplet; brs, broad singlet; dd, double of doublets. Analytical thin-layer chromatography (TLC) was carried out on silica gel F-254 plates (Merck). The solvents used in MS measures were acetone, acetonitrile (Chromasolv grade), purchased from Sigma-Aldrich, and milli-Q water 18 MX, obtained from Millipore's Simplicity system. The LC mass spectra were obtained using a 1200 L triple quadrupole system (Varian, Palo Alto, CA) equipped with an electron spray source (ESI) operating in both positive and negative ions.

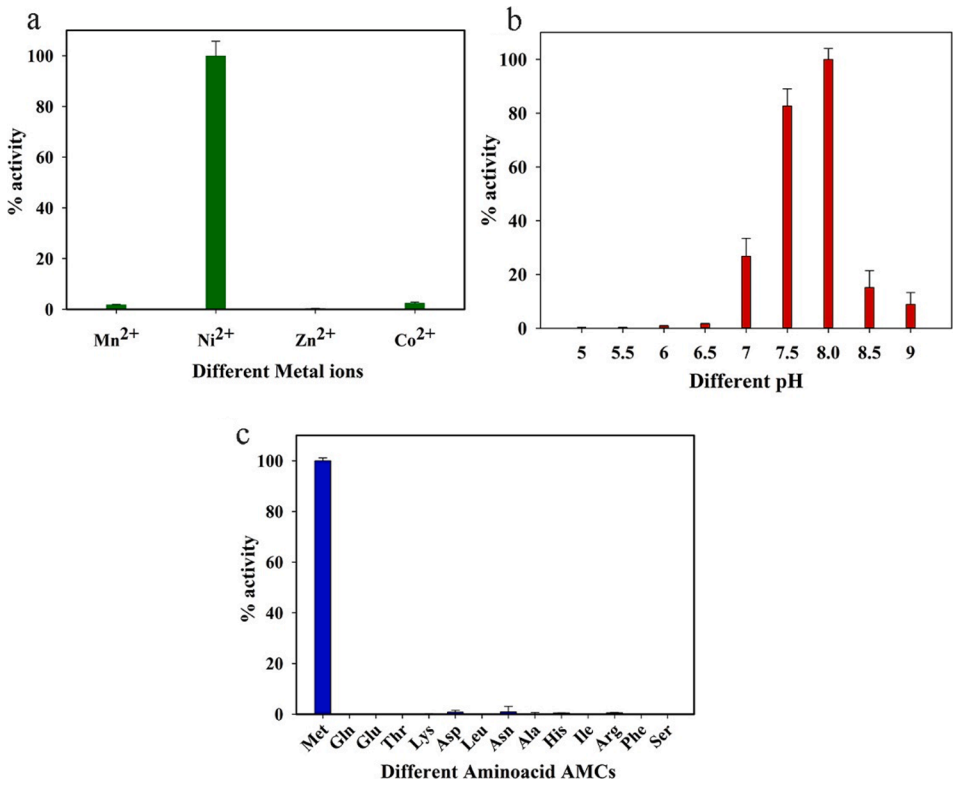

Fig. 3. a. Metal specificity of *Hp*MetAP1a towards Met-AMC. The best activity was observed with Ni^{2+}. b. The best activity of the *Hp*MetAP1a activity was shown at pH 8.0 towards Met-AMC. c. Substrate Specificity of *Hp*MetAP1a towards different amino acid-AMCs in percentage activity. *Hp*MetAP1a cleaves only methionine-AMC in the presence of $NiCl_2$ at pH 8.0.

2.12.1. Chemistry: Experimental protocols

2.12.1.1. General procedure for the synthesis of 7d4 and 7g7. Solvents and all the reagents were purchased from Sigma-Aldrich (India), Alfa Aesar (India), and TCI (India). Nuclear magnetic resonance spectra (^{1}H NMR: 400 MHz and ^{13}C NMR: 100 MHz) were recorded in $CDCl_3$ and DMSO-d_6 using an Avance III 400 MHz spectrometer (Bruker). Chemical shifts are reported in parts per million (ppm) and the coupling constants (J) are expressed in Hertz (Hz). Splitting patterns are designated as follows: s, singlet; d, doublet; t, triplet; q, quadruplet; m, multiplet; brs, broad singlet; dd, double of doublets. Analytical thin-layer chromatography (TLC) was carried out on silica gel F-254 plates (Merck). The solvents used in MS measures were acetone, acetonitrile (Chromasolv grade), purchased from Sigma-Aldrich, and Milli-Q water 18 MX, obtained from Millipore's Simplicity system. The LC mass spectra were obtained using a 1200 L triple quadrupole system (Varian, Palo Alto, CA) equipped with an electron spray source (ESI) operating in both positive and negative ions.

2.12.2. Preparation of target compounds

2.12.2.1. Synthesis of 1H-pyrrolo[2,3-b]pyridine-4-carbonitrile (2). To a solution of 4-bromo-1H-pyrrolo[2,3-*b*]pyridine (12 g, 60.91 mmol, 1 eq) in 80 mL of DMF in a sealed tube was added zinc cyanide (14.3 g, 121.83 mmol, 2 eq) at RT and the reaction mixture was purged with Argon for 15 min. Pd(Tetrakis) (3.52 g, 3.045 mmol, 0.05 eq) was added, and purging continued for 15 min more. The seal tube was closed and the reaction mixture was heated to 100 °C and stirred for 18 h. TLC showed completion of the reaction. The reaction mixture cooled to RT, quenched in 500 mL of ice-cold water with stirring, and extracted with ethyl acetate (3 × 100 mL). The combined organic layer was washed with water (50 mL), brine (50 mL), dried over Na_2SO_4, filtered, and concentrated to get the crude compound. The crude compound was purified by using flash column chromatography using 20% ethyl acetate in pet ether as a mobile phase. Collected solvent concentrated to get 8 g (yield: 92%) of 1H-pyrrolo[2,3-*b*]pyridine-4-carbonitrile as a pale orange solid. TLC: R_f: 0.4 (40% EtOAc in pet ether). LCMS (ESI positive) m/z = 143.9. LC Purity: 97.3%. ^{1}HNMR (400 MHz, DMSO-d_6): δ 12.36 (brs, 1H), 8.4 (d, J = 9.2 Hz, 1H), 7.83 (d, J = 1.2 Hz, 1H), 7.55 (d, J = 8.4 Hz, 1H), 6.65 (d, J = 1.6 Hz, 1H).

2.12.2.2. 1H-pyrrolo[2,3-b]pyridine-4-carboxylic acid (3). To a solution of 1H-pyrrolo[2,3-*b*]pyridine-4-carbonitrile (2) (8.4 g, 58.74 mmol, 1 eq) in 70 mL of ethanol was added 40 mL of an aqueous 20% KOH solution dropwise at RT. The reaction mixture was heated to 100 °C and stirred for 16 h. TLC showed completion of the reaction. The reaction mixture was cooled to RT and concentrated to remove ethanol under vacuum. The aqueous layer was diluted with 50 mL of water and washed with ethyl acetate (2 × 50 mL). The aqueous layer was acidified to pH 6 by using 1 M HCl. The precipitated solid was collected, washed with water, pet ether, and dried under a high vacuum to get 7.85 g (yield: 82.6%) of 1H-pyrrolo[2,3-*b*]pyridine-4-carboxylic acid as a pale yellow solid. TLC: R_f: 0.1(EtOAc). LCMS (ESI positive) m/z = 162.8. LC Purity: 99.1%. ^{1}HNMR (400 MHz, DMSO-d_6): δ 13.3 (brs, 1H), 11.9 (brs, 1H), 8.34 (d, J = 4.8 Hz, 1H), 7.65 (t, J = 2.8 Hz, 1H), 7.56 (d, J = 4.8 Hz, 1H) and 6.87 (m, 1H).

2.12.2.3. Methyl 1H-pyrrolo[2,3-b]pyridine-4-carboxylate (4). To an ice-cold solution of 1H-pyrrolo[2,3-*b*]pyridine-4-carboxylic acid (7.8 g, 48.14 mmol, 1 eq) in 150 mL of methanol was added thionyl chloride (14 mL, 192.6 mmol, 4 eq) dropwise. The reaction mixture was heated to reflux and stirred for 18 h. crude LCMS showed completion of the reaction. The reaction mixture cooled to RT and concentrated. The crude compound was dissolved in water (250 mL), pH adjusted to 12 by using 1 N NaOH solution. The precipitated solid was collected, washed with water (2 × 30 mL), pet ether (2 × 50 mL), and dried under a high

Table 2
Ki values of hydroxamic acid derivatives of azaindoles against *Hs*MetAP1b and *Hp*MetAP1a.

Compound code	Structure	*Hp*MetAP1a-Ki (μM)	*Hs*MetAP1b-Ki (μM)	Inhibition favoring the *Hp*MetAP1a
7d4	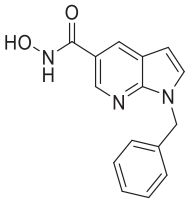	0.11 ± 0.010	57.33 ± 3.30	521.1
7g7	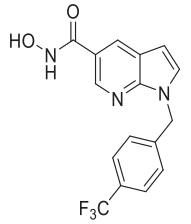	0.14 ± 0.050	57.58 ± 14.17	411.2
7c	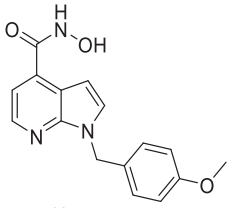	0.17 ± 0.096	34.42 ± 3.6	202.4
7g	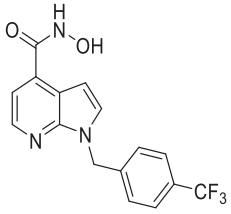	0.84 ± 0.35	135.9 ± 16.3	161.7
7e5	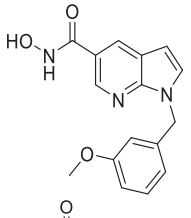	0.62 ± 0.096	36.61 ± 0.44	59.0
7i9	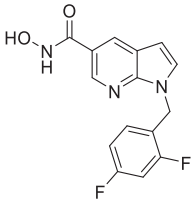	0.23 ± 0.079	10.79 ± 0.78	46.9
7f	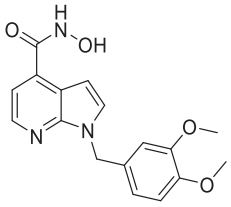	0.82 ± 0.154	36.59 ± 4.9	43.5
7c3	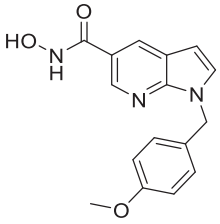	0.59 ± 0.106	13.76 ± 1.514	23.2
7d		0.53 ± 0.073	11.05 ± 1.92	20.84

(*continued on next page*)

Table 2 (*continued*)

Compound code	Structure	*Hp*MetAP1a-Ki (μM)	*Hs*MetAP1b-Ki (μM)	Inhibition favoring the *Hp*MetAP1a
7f6	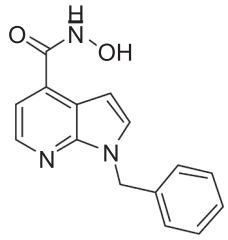	0.28 ± 0.007	5.427 ± 0.88	19.3
7a1	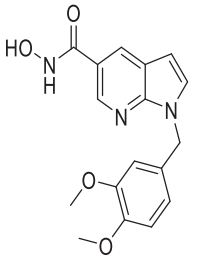	0.44 ± 0.054	8.18 ± 2.71	18.5
7j10	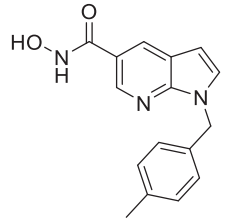	0.78 ± 0.072	10.07 ± 1.39	12.9
7a	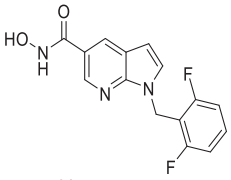	5.21 ± 0.72	60.37 ± 12.82	11.5
7h	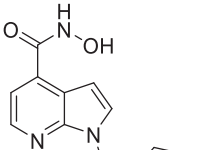	1.49 ± 0.370	8.656 ± 0.81	5.8
7b2	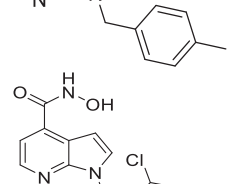	5.37 ± 0.696	22.41 ± 1.24	4.1
7e	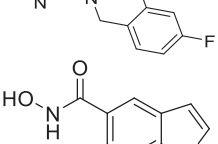	0.07 ± 0.024	ND	–
7b		1.17 ± 0.23	ND	–

(*continued on next page*)

Table 2 (*continued*)

Compound code	Structure	*Hp*MetAP1a-Ki (μM)	*Hs*MetAP1b-Ki (μM)	Inhibition favoring the *Hp*MetAP1a
	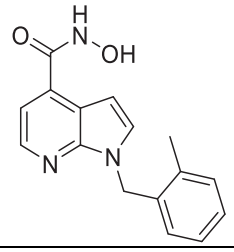			

ND – Not determined.

Table 3
Data collection and refinement statistics of *Hs*MetAP1b in complex with **7d** and **7e5.**

	*Hs*MetAP1b-**7d**	*Hs*MetAP1b-**7e5**
Cell parameters		
Space group	$P2_1$	$P2_1$
Unit cell (Å) (a, b, c)	47.55, 77.22, 48.65	47.57, 77.25, 48.62
α = γ = 90°, β (°)	91.549	91.54
Data collection[a]		
Resolution range (Å)[b]	47.53–1.35 (1.401–1.353)	40.5–1.29 (1.337–1.291)
Total reflections	519,285	580,633
Unique reflections[b]	75,652 (7550)	87,090 (8351)
Completeness[b] (%)	98.90 (99.16)	98.96 (95.44)
Mean I/sigma (I)	20.1	17.9
Multiplicity	6.8	6.6
R-merge (%)	4.2	4.7
R-meas (%)	4.6	5.1
Refinement statistics		
R-work (%)	18.99	18.40
R-free (%)	20.20	21.20
No. of non-H atoms	2646	2631
Macromolecule	2464	2436
Protein residues	304	304
Wilson B-factor	15.40	15.70
Average B-factor (Å^2)	28.00	25.00
Ramachandran favored (%)	98.90	98.34
Ramachandran allowed (%)	1.00	1.32
Ramachandran outliers (%)	0.37	0.33
R.M.S.D[c] (bonds) (Å)	0.018	0.025
R.M.S.D[c] (angles) (°)	2.26	2.29
Protein Data Bank code	6LZC	6LZB

[a] X-ray source: XRD2 beamline, Elettra Synchrotron Trieste, Italy.
[b] Statistics for the highest-resolution shell are shown in parentheses.
[c] RMSD, root mean square deviation.

vacuum to get 7.7 g (yield: 90.8%) of methyl 1H-pyrrolo[2,3-*b*]pyridine-4-carboxylate as pale yellow solid. TLC: R_f: 0.4 (EtOAc). LCMS (ESI positive) $m/z = 177$. LC Purity: 99.8%. ^{1}HNMR (400 MHz, DMSO-d_6): δ 10.1 (brs, 1H), 8.44 (d, $J = 4.8$ Hz, 1H), 7.74 (d, $J = 4.8$ Hz, 1H), 7.52 (t, 1H), 7.07 (t, 1H) and 4.03 (s, 3H).

2.12.3. Preparation of target compounds

2.12.3.1. 1H-pyrrolo[2,3-b]pyridine-5-carbonitrile (2a). To a solution of 5-bromo-1H-pyrrolo[2,3-*b*]pyridine **1a** (10 g, 51.02 mmol) in DMF in a sealed tube was added zinc cyanide (11.9 g, 102.04 mmol) at room temperature and the reaction mixture was purged with Argon for 15 min. Pd(Tetrakis) (2.9 g, 2.55 mmol) was added, and purging continued for 15 min more. The seal tube was closed and the reaction mixture was heated to 100 °C and stirred for 18 h and monitored by TLC. The reaction mixture cooled to room temperature, quenched in ice-cold water with stirring, and extracted with ethyl acetate. The combined organic layer was washed with water, brine, dried over anhydrous Na_2SO_4, filtered, and concentrated to get the crude compound. The crude compound was purified using flash column chromatography using 10% ethyl acetate in pet ether as mobile phase. Collected solvent concentrated to get 6.5 g (yield: 89.1%) as pale orange solid. TLC: R_f: 0.4 (40% EtOAc in pet ether). MS (ESI +) $C_8H_5N_3$ for m/z 143.9) $[M + H]^+$; LC purity 94.15%, (ret. time, 4.16 min); ^{1}H NMR (400 MHz, DMSO-d_6) δ 12.30 (brs, 1H), 8.58 (s, 1H), 8.50–8.49 (d, $J = 0.8$ Hz, 1H), 7.70–7.69 (m, 1H), 6.609–6.601 (s, 1H).

2.12.3.2. The general procedure of benzylation (5d4 and 5g7). To a solution of Methyl 1H-pyrrolo[2,3-b], pyridine-5-carboxylate **4a** in anhydrous DMF was added K_2CO_3 at room temperature and the reaction mixture was stirred for 30 min. To this was added dropwise benzyl bromide/ chloride and the reaction mixture was stirred for 16 h and monitored by TLC. The reaction mixture was quenched in ice-cold water and extracted with ethyl acetate (3 × 30 mL). The combined organic layer was washed with water, brine, dried over anhydrous Na_2SO_4, filtered, and concentrated to get the crude compound. The crude compound was purified by flash column chromatography (silica gel 230–400 mesh) using 0–20% ethyl acetate in pet ether as a mobile phase.

2.12.3.3. Methyl 1-benzyl-1H-pyrrolo[2,3-b]pyridine-5-carboxylate (5d4). Yield: 600 mg (95.6%) as pale yellow solid.; ^{1}H NMR (400 MHz, $CDCl_3$) δ 9.02–9.01 (s, $J = 4$ Hz, 1H), 8.59 (s, 1H), 7.31–7.20 (m, 6H), 6.58–6.57 (d, $J = 4$ Hz, 2H), 5.52 (s, 2H), 3.96 (s, 3H). MS (ESI +) $C_{16}H_{14}N_2O_2$ for m/z 267) $[M + H]^+$; LC purity 95.11%, (ret. time, 3.51 min).

2.12.3.4. Methyl 1-(4-(trifluoromethyl)benzyl)-1H-pyrrolo[2,3-b]pyridine-5-carboxylate (5g7). Yield: 411 mg (43.3%) as off white solid. ^{1}H NMR (400 MHz, $CDCl_3$) δ 9.01–9.00 (s, $J = 4$ Hz, 1H), 8.61–8.60 (s, 1H), 7.56 (d, $J = 4$ Hz, 1H), 7.54 (s, 1H), 7.30–7.28 (d, $J = 8$ Hz, 2H), 7.24–7.23 (d, $J = 4$ Hz, 1H), 6.62–6.62 (d, $J = 4$ Hz, 1H), 5.58 (s, 2H), 3.96 (s, 3H). MS (ESI +) $C_{17}H_{13}F_3N_2O_2$ for m/z 335.1) $[M + H]^+$; LC purity 95.99%, (ret. time, 3.75 min).

2.12.3.5. General procedure of hydrolysis (6d4 and 6g7). To an ice-cold solution of SM in THF: MeOH: water was added LiOH·H2O portion-wise. The reaction mixture was stirred for 16 h at RT. TLC showed completion of the reaction. The reaction mixture was concentrated to remove volatiles and diluted with water. The aqueous layer was washed with ethyl acetate and the aqueous layer was acidified to pH-2 using 1 N aqueous HCl. The precipitated solid was collected by filtration, washed with water, and dried under a high vacuum. The solid was triturated with ethyl acetate, decanted, and dried under a high vacuum to get the desired compound as a white solid.

2.12.3.6. 1-benzyl-1H-pyrrolo[2,3-b]pyridine-5-carboxylic acid (6d4). Yield: 360 mg (86.3%) as white solid. ^{1}H NMR (400 MHz, $CDCl_3$) δ 9.11 (s, 1H), 8.67 (s, 1H), 7.33–7.32 (d, $J = 4$ Hz, 1H), 7.28–7.22 (m, 5H), 6.62–6.61 (d, $J = 4$ Hz, 1H), 5.54 (s, 2H). MS (ESI +) $C_{15}H_{12}N_2O_2$ for m/z 253.1) $[M + H]^+$; LC purity 99.92%, (ret. time, 2.68 min).

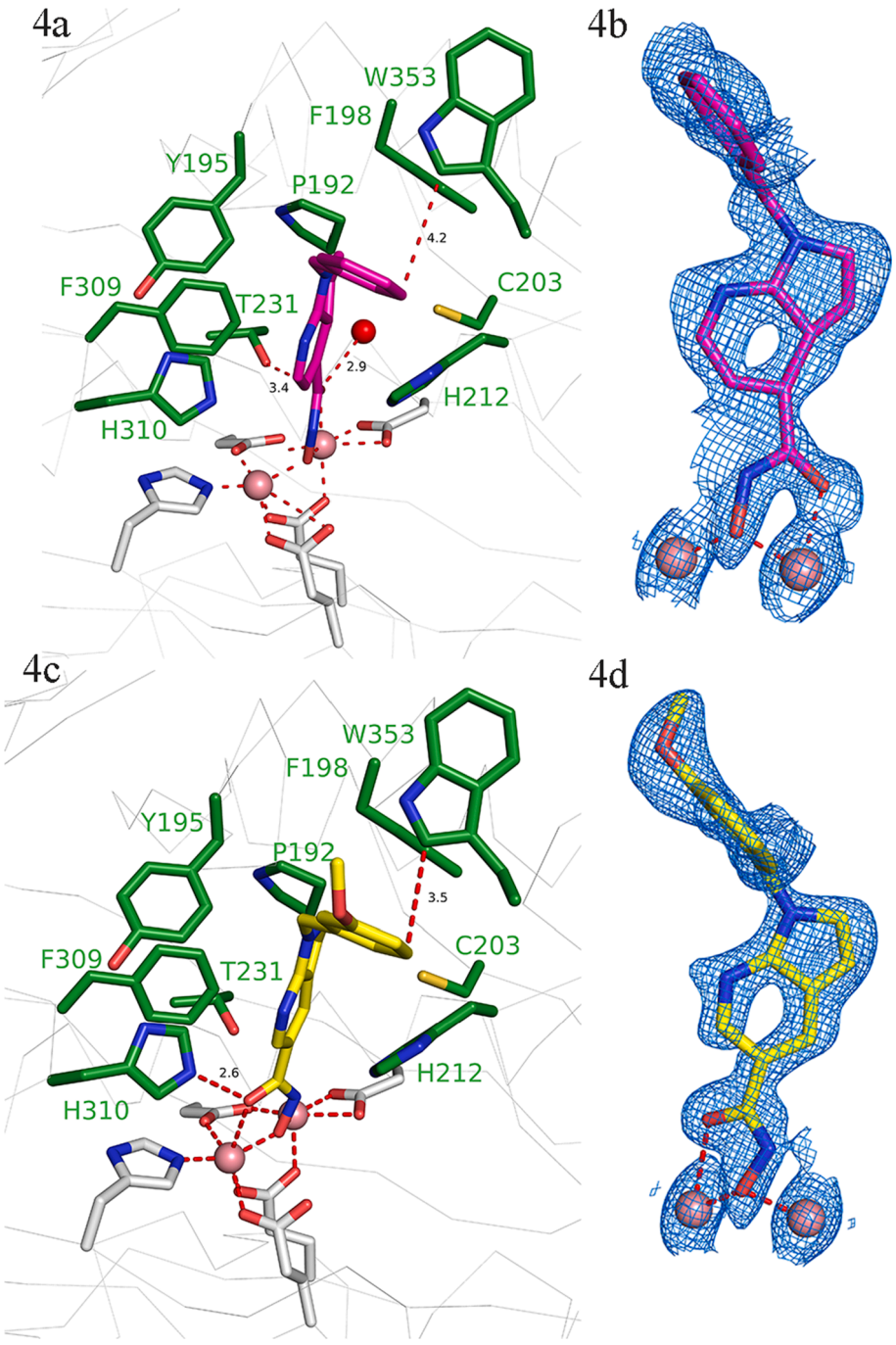

Fig. 4. a) *Hs*MetAP1b S1 pocket residues are shown in sticks (green) in complex with compound **7d** is shown in pink b) Hydroxamic acid moiety coordinates with the metal cofactors. c) *Hs*MetAP1b S1 pocket residues are shown in sticks (green) in complex with compound **7e5** shown in yellow. d) Hydroxamic acid moiety coordinates with the metal cofactors. (For interpretation of the references to colour in this figure legend, the reader is referred to the web version of this article.)

2.12.3.7. 1-(4-(trifluoromethyl)benzyl)-1H-pyrrolo[2,3-b]pyridine-5-carboxylic acid (6g7). Yield: 380 mg (79.3%) as white solid. MS (ESI +) $C_{16}H_{11}F_3N_2O_2$ for *m/z* 321.1) $[M + H]^+$; LC purity 99.91%, (ret. time, 5.32 min).

2.12.3.8. The general procedure of amide coupling (7d4 and 7g7). To a solution of **6a1** in anhydrous THF was added triethylamine, hydroxylamine hydrochloride at 0 °C and the reaction mixture was stirred for 30 min. To this was added HATU and the reaction mixture was stirred for 16 h and monitored by TLC. The reaction mixture filtered through a celite pad and filtrate evaporated under reduced pressure to get the crude compound. The crude compound was purified by flash column chromatography (silica gel 230–400 mesh) using 40–50% ethyl acetate in pet ether as a mobile phase. Collected solvent concentrated to get the desired compound as white solid.

2.12.3.9. 1-benzyl-N-hydroxy-1H-pyrrolo[2,3-b]pyridine-5-carboxamide (7d4). Yield: 63 mg (17%) as white solid. ^{1}H NMR (300 MHz, $CDCl_3$) δ 11.21 (s, 1H), 9.03 (s, 1H), 8.64 (s, 1H), 8.35–8.34 (d, $J = 1.8$ Hz, 1H), 7.72–7.71 (d, $J = 3.3$ Hz, 1H), 7.32–7.21 (m, 5H), 6.62–6.61 (d, $J = 3.6$ Hz, 1H), 5.50 (s, 2H). ^{13}C NMR (75 MHz, DMSO-D_6): δ 148.0, 141.8, 138.1, 130.71, 128.5, 127.7, 127.4, 127.2, 121.0, 119.1, 100.6, and 47.3. MS (ESI +) $C_{15}H_{13}N_3O_2$ for *m/z* 268.1) $[M + H]^+$; LC purity 99.08%, (ret. time, 3.93 min).

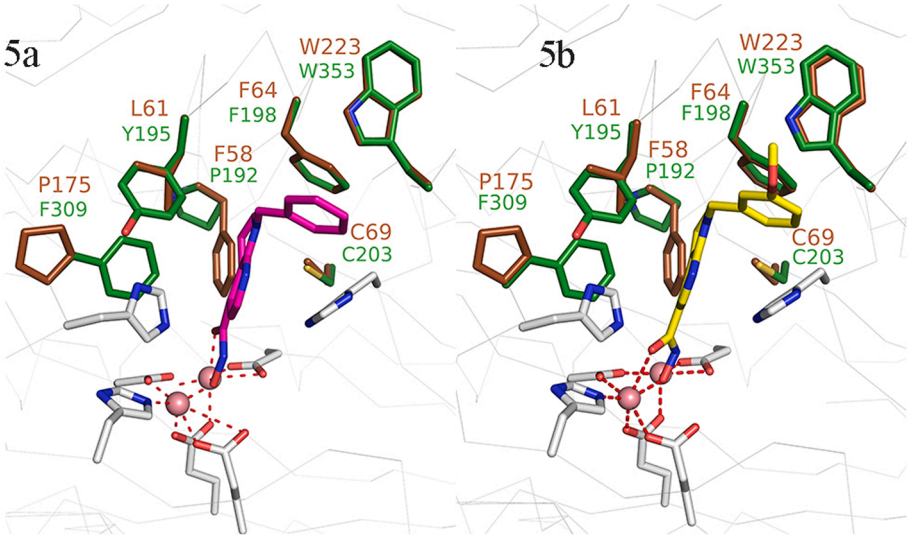

Fig. 5. a) Structural alignment of *Hs*MetAP1b (green) in complex with compound **7d** (pink) and *Hp*MetAP1a homology model (brown) b) Structural alignment of *Hs*MetAP1b (green) in complex with compound **7e5** (yellow) and *Hp*MetAP1a homology model (brown). (For interpretation of the references to colour in this figure legend, the reader is referred to the web version of this article.)

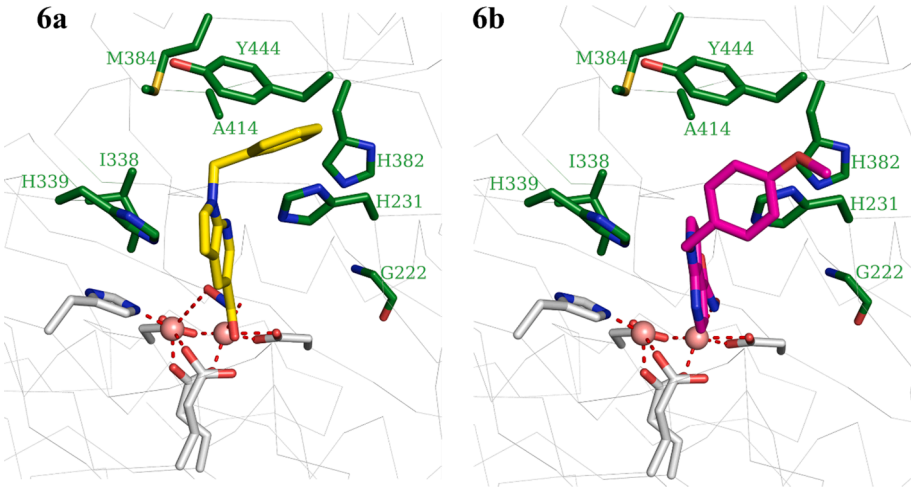

Fig. 6. a) Molecular modeling of **7d4** (yellow) in the active site of *Hs*MetAP2 (green). b) Molecular modeling of **7c** (pink) in the active site of *Hs*MetAP2 (green). Metal binding residues are shown in gray. (For interpretation of the references to colour in this figure legend, the reader is referred to the web version of this article.)

2.12.3.10. N-hydroxy-1-(4-(trifluoromethyl)benzyl)-1H-pyrrolo[2,3-b] pyridine-5-carboxamide (7g7). Yield: 80 mg (25.4%) as white solid. ^{1}H NMR (300 MHz, DMSO-D_6) δ 11.22 (s, 1H), 9.04 (s, 1H), 8.64–8.63 (d, J = 1.5 Hz, 1H), 8.37–8.36 (d, J = 1.5 Hz, 1H), 7.77–7.76 (m, 1H), 7.69–7.66 (m, 2H), 7.40–7.38 (m, 2H), 6.66–6.65 (d, J = 3.6 Hz, 1H), 5.62 (s, 2H). MS (ESI +) $C_{16}H_{12}F_3N_3O_2$ for m/z 336.1) $[M + H]^+$; LC purity 98.88%, (ret. time, 4.65 min).

3. Results and discussion

Since Type 1 MetAPs are recognized as drug targets against microbial infections, they have been studied extensively [12,16,41–43]. Several classes of inhibitors have been reported against these enzymes that include pyridyl pyrimidines, phosphonic acids, bengamides, hydroxamic acids, etc. [12,13,44–50]. One of the limitations of most of the reported inhibitors is the lack of selectivity. All earlier studies have been dedicated to understanding a single enzyme at a time based on the disease of interest and the inhibitors have been designed specifically for that enzyme. To the best of our knowledge, there is no report till date on understanding the variability of the active site Type 1 MetAP from their human counterpart. We believe that this understanding will allow scientists to study only those microbial enzymes that have appreciable differences from the human enzyme. In this study, we have analyzed 13 sets of 25 hundred sequence alignments that are based on homology driven secondary structure prediction (HSSP) [51]. For each protein of known 3D structure from the Protein Data Bank (PDB) [30], the database has a multiple sequence alignment of all available homologues and a sequence profile characteristic of the family. Each HSSP file contains a maximum of 2,500 homolog proteins with a lower limit of 30% sequence identity. However, there could be redundancy of protein sequences between each alignment, which we did not attempt to eliminate (Table 1 and Fig. 1).

Five residues (one histidine, two glutamates, and two aspartates) coordinate with the active site metal ions, while two other histidine residues are placed at either side of the entrance of the active site. All these seven residues are conserved among all MetAPs reported till date (Fig. 1). For the convenience of description, we divide the S1 pocket where the substrate methionine side chain binds into two halves, the left lobe and the right lobe that contain three residues each. Three residues in the right lobe of the S1 pocket of human MetAP1b are F198, C203,

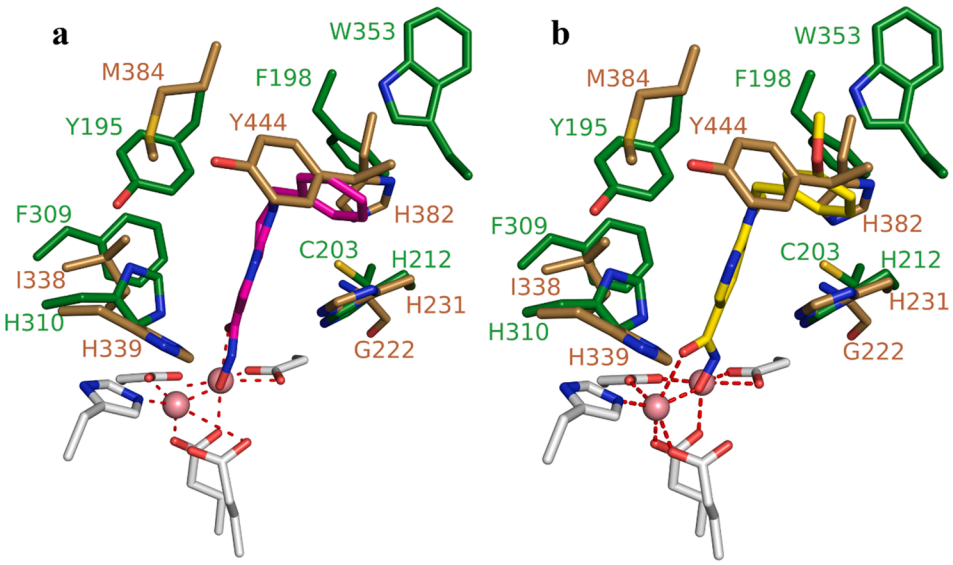

Fig. 7. a) Structural alignment of *Hs*MetAP1b (green) in complex with compound **7d** (pink) and *Hs*MetAP2 (PDB ID:2ADU) (brown) b) Structural alignment of *Hs*MetAP1b (green) in complex with compound **7e5** (yellow) and *Hs*MetAP2 (PDB ID:2ADU) (brown). Metal binding residues are shown in gray. (For interpretation of the references to colour in this figure legend, the reader is referred to the web version of this article.)

and W353. Based on the 13 alignment files, tryptophan is conserved 100% among all Type 1 MetAPs while the F198 position is either phenylalanine (73.5%) or a tyrosine (26.5%). Similarly, the C203 position is occupied by cysteine at 97%, asparagine at 2.5%, while the other 0.5% is occupied by leucine, threonine, and valine. Compared to the right lobe of the S1 pocket, the left lobe is more variable. In the human MetAP1b, these residues are P192, Y195 and F309 labeled as Site 1, Site 2, and Site 3 in Fig. 1. Site 1 is most variable in the left lobe of the S1 pocket represented by P(40.7%), F(19.2%), Y(16.3%), N(5%), T (4.6%), L(3.5%), Q(3.4%), S(2.7%), C(2.2%), E(1.5%) and few others in less than 1% each. Site 2 ranks second in variation substituted by Y (72.4%), P (5.5%), T (5.1%), C (3.6%), G (3%), N (2%), F (1.9%) and V (1%). Site 3 is substituted by F (59.3%), M (17%), L (12.8%), Y (5.3%), I (2.3%) and V (1.3%) (Table 1 and Fig. 1).

Recently, we have developed species-specific inhibitors based on the variation of Site 3 [12]. F309 in the *Hs*MetAP1b is represented by a methionine in *S. pneumoniae* MetAP1a' (*Sp*MetAP1a'). This single amino acid difference was sufficient to discover selective inhibitors *Sp*MetAP1a' [12]. Similarly, ovalicin inhibits Type 2 MetAPs by a million-fold compared to the Type 1 MetAPs from *E. coli* and human which have phenylalanine at Site 2. Nanomolar inhibition is noticed in Type 1 enzymes like *Sp*MetAP1a', where phenylalanine is replaced by methionine [27].

Column 2 describes the variation of residues at Site-1, Site2, and Site-3 of the left lobe of the MetAP active site and column 3 describes the conservation of residues at the right lobe of the MetAP active site.

3.1. Sequence and structural comparison of HpMetAP1a with human MetAP1b:

The protein sequence of *HpMetAP1a* is 32.7% identical to human MetAP1b (**Fig. S3**). It is important to note that the human MetAP1b used in this study is devoid of *N*-terminal zinc fingers as reported earlier [12]. 3D model of the *Hp*MetAP1a was developed and validated by RAMPAGE [36]. Structural alignment between the human (PDB ID: 4U6J) and pylori MetAPs is performed using Clustal Omega [52]. As expected, the left side of the S1 pocket is more varied in the *Hp*MetAP1a in comparison with the human enzyme. P192, Y195, and F309 in Site 1, Site 2, and Site 3, respectively in human MetAP are replaced by F58, L61, and P175 in *pylori* enzyme, while all three residues in the right lobe are absolutely conserved between the two (Fig. 2). We note that the position of a proline and a phenylalanine were switched between the proteins at site 1 and site 2. The bulky aromatic Y195 in the human enzyme is replaced by a relatively smaller amino acid (L61) in the pylori enzyme making the S1 pocket wider in the later. Based on these fine differences, we believe that the inhibitors designed will show differential inhibition against the *H. pylori* and human MetAPs.

3.2. Design and synthesis of hydroxamic acid-based azaindoles

Hydroxamic acid is a well-known metal chelating moiety used in the design of inhibitors against several metalloproteases [22,45,46,53,54]. Since both the aromatic residues as in human MetAP1b at Site 2 and Site 3 are truncated to smaller amino acids (leucine and proline, respectively) in *Hp*MetAP1a in the left lobe, an extra space is created. Using this understanding, we designed azaindole derivatives with two substitution points. We analyzed that the aromatic groups at Site 2 and Site 3 in the human enzyme would resist the binding of these molecules. To optimize the binding, we varied the hydroxamic acid on the 4th (**7a-7h**) and 5th (**7a1-7j10**) positions of the azaindole ring. In addition, an aromatic ring with different substitutes has been added in all compounds at position 1. Substitutions on the aromatic group in compounds **7a-7g** are repeated in compounds **7a1-7g7** and in the same order. Together, we synthesized 17 molecules.

3.3. Cloning, expression, purification, and characterization of HpMetAP1a and HsMetAP1b

Human MetAP1b used in this study was prepared as reported earlier [12,13,27,55]. *Hp*MetAP1a was cloned into pET15b vector. Both proteins were expressed and purified to homogeneity (**Fig. S2**). Both the proteins were inactive after purification. Enzymes were activated after the addition of transition metal ions. MetAPs are metalloproteases with variable specificity to first-row transition metal ions. Most of the MetAPs prefer Co^{2+} better than others, including the human Type 1 enzyme. Surprisingly, *Hp*MetAP1a displayed activity in the presence of $NiCl_2$ and negligible activity with other metal ions (Fig. 3**a**). Using Ni^{2+} as a co-factor, the pylori enzyme had optimum activity at pH 8.0 (Fig. 3**b**). Among all the tested AMC attached amino acids, only Met-AMC was hydrolyzed (Fig. 3**c**). All further enzyme kinetic and inhibition studies for *Hp*MetAP1a were carried out with Ni^{2+} as co-factor at pH 8.0 and Met-AMC as substrate. K_M and k_{cat} for *Hp*MetAP1a were determined as

94.17 ± 6.8 μM and 298.50 sec^{-1}, respectively (**Table S2**).

3.4. Selective inhibition of Helicobacter pylori MetAP1a compared to its human counterpart

The library of 17 compounds synthesized in this study were screened for inhibition and determined their inhibition constants (*K*i) against pylori and human Type 1 MetAPs (Table 2). As we hypothesized from the design, all 17 molecules inhibited the pylori enzyme with high selectivity compared to the human enzyme. Of the eight 4-azaindole substituted compounds, five showed inhibition better than 1 μM against *Hp*MetAP1a, while eight out of nine 5-azaindole substituted compounds showed lower activity than 1 μM. The best compound in the 4-substituted series (**7c**) showed 200-fold selective inhibition of pylori enzyme compared to human MetAP1b. Among the 5-substituted series, **7d4** showed 520 folds and **7g7** showed 400-fold selectivity against *Hp*MetAP1a. Among the substituents of the aromatic rings at the 1st position on the azaindole, compounds with trifluoromethyl groups (**7g** and **7g7**) are better inhibitors with more than 100-fold selectivity. Surprisingly, the best molecule with more than 500-fold selectivity has no substitution on the aromatic ring (**7d4**). Compound **7i9** with two fluorine atoms at position 2 and 4 though inhibit the *Hp*MetAP1a at a low concentration similar to **7j10**, it also inhibits the human enzyme at low concentration (*K*i = 10.07 μM). Compound **7d** inhibits the *Hp*MetAP1a at 0.53 μM and human MetAP1b at 11.05 μM. On the other hand, homologous compound, **7d4** inhibits at 0.11 μM and 57.33 μM, pylori, and human MetAPs respectively. Together, the structure activity relationship analysis suggests that azaindoles with hydroxamic acid at the 4th position and aromatic rings with halogen substitution at position 1 are better and selective inhibitors against *Hp*MetAP1a (Table 2).

3.5. Crystal structure of inhibitors in complex with human enzyme

Several attempts to crystallize the *Hp*MetAP1a were not successful. To get a clue on the mode of binding, we have determined the crystal structure of two inhibitors in complex with human enzyme using the reported conditions (Table 3) [12]. Several inhibitors were soaked but crystals in complex with compounds **7d** (4-azaindole derivative) and **7e5** (5-azaindole derivative) yielded the diffraction quality crystals. The overall structure of inhibitor complexes is similar to the human holo-structure (PDB ID: 2B3H) with less than 0.15 Å RMSD (all main chain atoms). Except for W353 all other amino acids in the active site are unaltered. Tryptophan side chain flips away by 180° to make space for the aromatic ring of the inhibitor. In compound **7d**, the hydroxamic acid at 4th position of the azaindole moiety binds to the bimetalo center placing the hydroxyl group between the two metal ions (Fig. 4**a and 4b**). In the holo structure, a water molecule acts as a bridge between the two metal ions that are believed to act as a nucleophile in hydrolyzing the peptide substrates. The ketone in the hydroxamic acid replaces another conserved water molecule and makes interactions with one of the metal ions in the metal center (2.3 Å) while making two other hydrogen bonds (T231 (3.4 Å) and a water molecule (2.9 Å)). The azaindole moiety extends into the hydrophobic S1 pocket formed by Y195, F198, H212, F309, and W253 (Fig. 4**a and 4b**). The benzyl group at N-1 pushes the W353 away by flipping it compared to the native position. In the new position, W353 makes edge-π interaction (4.2 Å) with the inhibitor on one side and partially solvent exposed on the other.

The overall conformation of the inhibitor in the *Hs*MetAP1b-**7e5** is similar to that of **7d** in *Hs*MetAP1b-**7d** except for the orientation of the carbonyl group in the hydroxamic moiety at the metal center (Fig. 4**c** and Fig. 4**d**). In this structure, the carbonyl group flips out and makes strong contact with H310 (2.6 Å). The rest of the molecule adopts a similar conformation including the flipping of the W353 side chain.

3.6. Comparison of binding of inhibitors with H. Pylori MetAP1a

To understand the structural basis for the selective inhibition of *H. pylori* MetAP1a, we have developed the 3D model of the full-length protein and compared it with the *Hs*MetAP1b-**7d** and *Hs*MetAP1b-**7e5** structures. *H. pylori* MetAP1a and the human MetAP1b share 32.7% identity with all-metal binding and gatekeeper histidines conserved. Of the six residues that make up the S1 pocket, all three residues in the right lobe are conserved (F198, C203, and W353 in humans and F64, C69, and W223 in the *H. pylori* protein). However as seen in other proteins described in Table 1, all residues in the left lobe are different in *Hp*MetAP1a (F58, L61, and P175) compared to the human counterpart (P192, Y195, and F309). It is important to note that in 2,500 sequences aligned with the human enzyme in the HSSP database as discussed above, there was no sequence with leucine at Site 2 and proline in Site 3. In the *Hs*MetAP1b-**7d** and *Hs*MetAP1b-**7e5**, methylene carbon of the benzyl group in inhibitors makes a very short contact with the side chain of the Y195 (3.4 Å). In the *H. pylori* MetAP1a, leucine being small and branched could rotate away with ease without affecting the neighboring residues thereby accommodating the inhibitor with better ease compared to that in the human enzyme thus providing the structural basis for selectivity (Fig. 5**a and 5b**). In this process, tryptophan (W223) may not have to flip away from the active site which could be costly in terms of energy.

3.7. In-silico analysis for the binding of azaindole hydroxamic acid derivatives on human Type 2 MetAP

We have carried our docking studies to understand whether azaindole derivatives non-specifically target human Type 2 MetAP (MetAP2) (Fig. 6 and Fig. 7). The major interaction of metal chelating inhibitors is their ability to interact strongly with metal ions in the active site. The active site of MetAP2 is having two histidine residues (H339, H231) which might be helping the enzyme in specificity. These two histidine residues are restricting the metal ion access for the bulky azaindole molecules used in this study.

4. Conclusions

We have identified MetAP1a from *Helicobacter pylori* that have variations within the S1 pocket, identified as left lobe compared to human MetAP1b. Using these differences in the active site we have designed and synthesized a library of 17 compounds that contain hydroxamic acid moiety as a metal binding scaffold. All 17 compounds inhibited the *pylori* enzyme with selectivity as high as 500 compared to the human enzyme. The crystal structure of the human enzyme with two compounds provided the molecular basis for selective inhibition.

Declaration of Competing Interest

The authors declare that they have no known competing financial interests or personal relationships that could have appeared to influence the work reported in this paper.

Acknowledgments

AA (EMR/2015/000461 and CRG/2019/006013) and RG (ECR/2016/000288) thank Science and Engineering Research Board (SERB), India for funding. RG acknowledges the lab facility at GITAM University. SCB and BK acknowledge fellowship from DBT (Department of Biotechnology), India. We acknowledge funding from DST (Department of Science and Technology), India for the transport of our crystals and data collection at Elettra Synchrotron. We thank Dr. Babu Manjashetty, Beamline Scientist, Elettra Synchrotron for collecting data on our behalf. The communication number issued by CSIR-IICT for this article is IICT/Pubs./2021/021.

Author contributions

AA and RG conceptualized and supervised the study and reviewed the manuscript. SCB performed all the experiments, analyzed the data, and drafted the manuscript. KV, AK, and OVS had synthesized the compounds and drafted the chemistry part. RVS and BK helped during crystallization trials of proteins.

Enzyme

Methionine aminopeptidase (EC: 3.4.11.18)

Databases

Structural data are available in PDB under accession numbers 6LZC, 6LZB.

Funding sources and disclosure of conflicts of interest

Funding agencies have no role in study design, in the collection, analysis, and interpretation of data; in the writing of the report; and in the decision to submit the article for publication.

Appendix A. Supplementary data

Supplementary data to this article can be found online at https://doi.org/10.1016/j.bioorg.2021.105185.

References

[1] M. Kozak, Initiation of translation in prokaryotes and eukaryotes, Gene 234 (2) (1999) 187–208.
[2] C. Giglione, T. Pierre, M. Fau-Meinnel, T. Meinnel, Peptide deformylase as a target for new generation, broad spectrum antimicrobial agents, *Mol. Microbiol.* 36 (6) (2000) 1197–1205.
[3] R.A. Bradshaw, W.W. Brickey, K.W. Walker, N-terminal processing: the methionine aminopeptidase and N alpha-acetyl transferase families, Trends Biochem. Sci. 23 (7) (1998) 263–267.
[4] J.A. Vetro, B. Dummitt, Y.-H. Chang, Methionine Aminopeptidase, in: N. M. Hooper, U. Lendeckel (Eds.), Aminopeptidases in Biology and Disease, Springer, US, Boston, MA, 2004, pp. 17–44.
[5] R. Bingel-Erlenmeyer, R. Kohler, G. Kramer, A. Sandikci, S. Antolić, T. Maier, C. Schaffitzel, B. Wiedmann, B. Bukau, N. Ban, A peptide deformylase-ribosome complex reveals mechanism of nascent chain processing, Nature 452 (7183) (2008) 108–111.
[6] J. Solbiati, A. Chapman-Smith, J.L. Miller, C.G. Miller Jr., J.E. Cronan Jr., Processing of the N termini of nascent polypeptide chains requires deformylation prior to methionine removal, J. Mol. Biol. 290 (3) (1999) 607–614.
[7] S.G. Bernier, N. Taghizadeh, C.D. Thompson, W.F. Westlin, G. Hannig, Methionine aminopeptidases type I and type II are essential to control cell proliferation, J. Cell. Biochem. 95 (6) (2005) 1191–1203.
[8] X. Li, Y.H. Chang, Amino-terminal protein processing in Saccharomyces cerevisiae is an essential function that requires two distinct methionine aminopeptidases, Proc. Natl. Acad. Sci. U. S. A. 92 (26) (1995) 12357–12361.
[9] J.J. Alvarado, A. Nemkal, J.M. Sauder, M. Russell, D.E. Akiyoshi, W. Shi, S.C. Almo, L.M. Weiss, Structure of a microsporidian methionine aminopeptidase type 2 complexed with fumagillin and TNP-470, Mol. Biochem. Parasitol. 168 (2) (2009) 158–167.
[10] C.M. Brdlik, C.M. Crews, A single amino acid residue defines the difference in ovalicin sensitivity between type I and II methionine aminopeptidases, J. Biol. Chem. 279 (10) (2004) 9475–9480.
[11] C. Giglione, S. Fieulaine, T. Meinnel, N-terminal protein modifications: Bringing back into play the ribosome, Biochimie 114 (1638–6183) (2015) 134–146.
[12] T. Arya, R. Reddi, C. Kishor, R.J. Ganji, S. Bhukya, R. Gumpena, S. McGowan, M. Drag, A. Addlagatta, Identification of the molecular basis of inhibitor selectivity between the human and streptococcal type I methionine aminopeptidases, J. Med. Chem. 58 (5) (2015) 2350–2357.
[13] C. Kishor, T. Arya, R. Reddi, X. Chen, V. Saddanapu, A.K. Marapaka, R. Gumpena, D. Ma, J.O. Liu, A. Addlagatta, Identification, biochemical and structural evaluation of species-specific inhibitors against type I methionine aminopeptidases, J. Med. Chem. 56 (13) (2013) 5295–5305.
[14] M.K. Haldar, M.D. Scott, N. Sule, D.K. Srivastava, S. Mallik, Synthesis of barbiturate-based methionine aminopeptidase-1 inhibitors, Bioorg. Med. Chem. Lett. 18 (7) (2008) 2373–2376.
[15] T.R. Helgren, P. Wangtrakuldee, B. Staker, T.J. Hagen, Advances in Bacterial Methionine Aminopeptidase Inhibition, Curr. Top Med. Chem. 16 (4) (2016) 397–414.
[16] Travis R. Helgren, Phumvadee Wangtrakuldee, Bart L. Staker, Timothy J. Hagen, Advances in Bacterial Methionine Aminopeptidase Inhibition, Curr. Top. Med. Chem. 16 (4) (2015) 397–414.
[17] V. Pillalamarri, T. Arya, N. Haque, S.C. Bala, A.K. Marapaka, A. Addlagatta, Discovery of natural product ovalicin sensitive type 1 methionine aminopeptidases: molecular and structural basis, Biochem. J. 476 (6) (2019) 991–1003.
[18] Sandeep Chowdary Bala, Neshatul Haque, Vijaykumar Pillalamarri, Ravikumar Reddi, Rajnandani Kashyap, Anil Kumar Marapaka, Anthony Addlagatta, Discovery of a new class of type 1 methionine aminopeptidases that have relaxed substrate specificity, Int. J. Biol. Macromol. 129 (2019) 523–529.
[19] R. Reddi, T. Arya, C. Kishor, R. Gumpena, R.J. Ganji, S. Bhukya, A. Addlagatta, Selective targeting of the conserved active site cysteine of Mycobacterium tuberculosis methionine aminopeptidase with electrophilic reagents, FEBS J. 281 (18) (2014) 4240–4248.
[20] C. Kishor, R. Gumpena, R. Reddi, A. Addlagatta, Structural studies of Enterococcus faecalis methionine aminopeptidase and design of microbe specific 2,2[prime or minute]-bipyridine based inhibitors, MedChemComm 3 (11) (2012) 1406–1412.
[21] Saleem Yousuf Bhat, Sonal Bhandari, Pavitra Suresh Thacker, Mohammed Arifuddin, Insaf Ahmed Qureshi, Development of quinoline-based hybrid as inhibitor of methionine aminopeptidase 1 from Leishmania donovani, Chem. Biol. Drug Des. 97 (2) (2021) 315–324.
[22] Natalie B. Vinh, Nyssa Drinkwater, Tess R. Malcolm, Michael Kassiou, Leonardo Lucantoni, Peter M. Grin, Georgina S. Butler, Sandra Duffy, Christopher M. Overall, Vicky M. Avery, Peter J. Scammells, Sheena McGowan, Hydroxamic acid inhibitors provide cross-species inhibition of Plasmodium M1 and M17 aminopeptidases, J. Med. Chem. 62 (2) (2019) 622–640.
[23] Travis R. Helgren, Elif S. Seven, Congling Chen, Thomas E. Edwards, Bart L. Staker, Jan Abendroth, Peter J. Myler, James R. Horn, Timothy J. Hagen, The identification of inhibitory compounds of Rickettsia prowazekii methionine aminopeptidase for antibacterial applications, Bioorg. Med. Chem. Lett. 28 (8) (2018) 1376–1380.
[24] Komagal Kannan Sivaraman, Alessandro Paiardini, Marcin Sieńczyk, Chiara Ruggeri, Christine A. Oellig, John P. Dalton, Peter J. Scammells, Marcin Drag, Sheena McGowan, Synthesis and structure-activity relationships of phosphonic arginine mimetics as inhibitors of the M1 and M17 aminopeptidases from Plasmodium falciparum, J. Med. Chem. 56 (12) (2013) 5213–5217.
[25] B.A. Salih, Helicobacter pylori infection in developing countries: the burden for how long? Saudi J. Gastroenterol. 15 (3) (2009) 201–207.
[26] M. Safavi, R. Sabourian, A. Foroumadi, Treatment of Helicobacter pylori infection: Current and future insights, World J. Clin. Cases 4 (1) (2016) 5–19.
[27] V. Pillalamarri, T. Arya, Discovery of natural product ovalicin sensitive type 1 methionine aminopeptidases: molecular and structural basis, Biochem. J. 476 (6) (2019) 991–1003.
[28] R.A. Copeland, Enzymes, A Practical Introduction to Structure, Mechanism, and Data Analysis, Wiley, 2004.
[29] Karine M. Sparta, Michael Krug, Udo Heinemann, Uwe Mueller, Manfred S. Weiss, XDSAPP2.0, J. Appl. Cryst 49 (3) (2016) 1085–1092.
[30] H.M. Berman, J. Westbrook, Z. Feng, G. Gilliland, T.N. Bhat, H. Weissig, I. N. Shindyalov, P.E. Bourne, The Protein Data Bank, Nucleic Acids Res. 28 (1) (2000) 235–242.
[31] Garib N. Murshudov, Pavol Skubák, Andrey A. Lebedev, Navraj S. Pannu, Roberto A. Steiner, Robert A. Nicholls, Martyn D. Winn, Fei Long, Alexei A. Vagin, REFMAC5 for the refinement of macromolecular crystal structures, Acta Crystallogr. D Biol. Crystallogr. 67 (4) (2011) 355–367.
[32] M.D. Winn, C.C. Ballard, K.D. Cowtan, E.J. Dodson, P. Emsley, P.R. Evans, R. M. Keegan, E.B. Krissinel, A.G. Leslie, A. McCoy, S.J. McNicholas, G.N. Murshudov, N.S. Pannu, E.A. Potterton, H.R. Powell, R.J. Read, A. Vagin, K.S. Wilson, Overview of the CCP4 suite and current developments, Acta Crystallogr. D Biol. Crystallogr. 67 (Pt 4) (2011) 235–242.
[33] P. Emsley, B. Lohkamp, W.G. Scott, K. Cowtan, Features and development of Coot, Acta Crystallogr. D Biol. Crystallogr. 66 (Pt 4) (2010) 486–501.
[34] L.L.C. Schrodinger, The PyMOL Molecular Graphics System, Version 1 (2015) 8.
[35] A. Waterhouse, M. Bertoni, S. Bienert, G. Studer, G. Tauriello, R. Gumienny, F. T. Heer, T.A.P. de Beer, C. Rempfer, L. Bordoli, R. Lepore, T. Schwede, SWISS-MODEL: homology modelling of protein structures and complexes, Nucleic Acids Res. 46 (W1) (2018) W296–W303.
[36] S.C. Lovell, I.W. Davis, W.B. Arendall 3rd, P.I. de Bakker, J.M. Word, M.G. Prisant, J.S. Richardson, D.C. Richardson, Structure validation by Calpha geometry: phi, psi and Cbeta deviation, Proteins 50 (3) (2003) 437–450.
[37] L.S. Kallander, Q. Lu, W. Chen, T. Tomaszek, G. Yang, D. Tew, T.D. Meek, G. A. Hofmann, C.K. Schulz-Pritchard, W.W. Smith, C.A. Janson, M.D. Ryan, G.-F. Zhang, K.O. Johanson, R.B. Kirkpatrick, T.F. Ho, P.W. Fisher, M.R. Mattern, R. K. Johnson, M.J. Hansbury, J.D. Winkler, K.W. Ward, D.F. Veber, S.K. Thompson, 4-Aryl-1,2,3-triazole: A Novel Template for a Reversible Methionine Aminopeptidase 2 Inhibitor, Optimized To Inhibit Angiogenesis in Vivo, J. Med. Chem. 48 (18) (2005) 5644–5647.
[38] A.W. Schüttelkopf, D.M. van Aalten, PRODRG: a tool for high-throughput crystallography of protein-ligand complexes, Acta Crystallogr. D Biol. Crystallogr. 60 (Pt 8) (2004) 1355–1363.
[39] O. Trott, A.J. Olson, AutoDock Vina: improving the speed and accuracy of docking with a new scoring function, efficient optimization, and multithreading, J. Comput. Chem. 31 (2) (2010) 455–461.
[40] G.M. Morris, R. Huey, W. Lindstrom, M.F. Sanner, R.K. Belew, D.S. Goodsell, A. J. Olson, AutoDock4 and AutoDockTools4: Automated docking with selective receptor flexibility, J. Comput. Chem. 30 (16) (2009) 2785–2791.

[41] C. Oefner, A. Douangamath, A. D'Arcy, S. Hafeli, D. Mareque, A. Mac Sweeney, J. Padilla, S. Pierau, H. Schulz, M. Thormann, S. Wadman, G.E. Dale, The 1.15A crystal structure of the Staphylococcus aureus methionyl-aminopeptidase and complexes with triazole based inhibitors, J. Mol. Biol. 332 (1) (2003) 13–21.
[42] Sergio C. Chai, Wen-Long Wang, De-Rong Ding, Qi-Zhuang Ye, Growth inhibition of Escherichia coli and methicillin-resistant Staphylococcus aureus by targeting cellular methionine aminopeptidase, Eur. J. Med. Chem. 46 (8) (2011) 3537–3540.
[43] V. Pillalamarri, C.G. Reddy, S.C. Bala, A. Jangam, V.V. Kutty, A. Addlagatta, Methionine aminopeptidases with short sequence inserts within the catalytic domain are differentially inhibited: Structural and biochemical studies of three proteins from Vibrio spp, Eur. J. Med. Chem. 209 (2021) 112883.
[44] Mir Mohammad Masood, Vijay K. Pillalamarri, Mohammad Irfan, Babita Aneja, Mohamad Aman Jairajpuri, Md. Zafaryab, M. Moshahid A. Rizvi, Umesh Yadava, Anthony Addlagatta, Mohammad Abid, Diketo acids and their amino acid/dipeptidic analogues as promising scaffolds for the development of bacterial methionine aminopeptidase inhibitors, RSC Adv. 5 (43) (2015) 34173–34183.
[45] X. Hu, J. Zhu, S. Srivathsan, D. Pei, Peptidyl hydroxamic acids as methionine aminopeptidase inhibitors, Bioorg. Med. Chem. Lett. 14 (1) (2004) 77–79.
[46] F. Huguet, A. Melet, R. Alves de Sousa, A. Lieutaud, J. Chevalier, L. Maigre, P. Deschamps, A. Tomas, N. Leulliot, J.-M. Pages, I. Artaud, Hydroxamic acids as potent inhibitors of Fe(II) and Mn(II) E. coli methionine aminopeptidase: biological activities and X-ray structures of oxazole hydroxamate-EcMetAP-Mn complexes, ChemMedChem 7 (6) (2012) 1020–1030.
[47] J.P. Lu, X.H. Yuan, Q.Z. Ye, Structural analysis of inhibition of Mycobacterium tuberculosis methionine aminopeptidase by bengamide derivatives, Eur. J. Med. Chem. 47 (1) (2012) 479–484.
[48] Jing-Ping Lu, Xiu-Hua Yuan, Hai Yuan, Wen-Long Wang, Baojie Wan, Scott G. Franzblau, Qi-Zhuang Ye, Inhibition of Mycobacterium tuberculosis methionine aminopeptidases by bengamide derivatives, ChemMedChem 6 (6) (2011) 1041–1048.
[49] Pengtao Zhang, Xinye Yang, Feiran Zhang, Sandra B. Gabelli, Renxiao Wang, Yihua Zhang, Shridhar Bhat, Xiaochun Chen, Manuel Furlani, L. Mario Amzel, Jun O. Liu, Dawei Ma, Pyridinylpyrimidines selectively inhibit human methionine aminopeptidase-1, Bioorg. Med. Chem. 21 (9) (2013) 2600–2617.
[50] D.H. Quan, G. Nagalingam, I. Luck, N. Proschogo, V. Pillalamarri, A. Addlagatta, E. Martinez, V. Sintchenko, P.A.-O. Rutledge, J.A. Triccas, Bengamides display potent activity against drug-resistant Mycobacterium tuberculosis, Sci. Rep. 9 (1) (2019) 14396.
[51] R. Schneider, A. de Daruvar, C. Sander, The HSSP database of protein structure-sequence alignments, Nucleic Acids Res. 25 (1) (1997) 226–230.
[52] F. Sievers, A. Wilm, D. Dineen, T.J. Gibson, K. Karplus, W. Li, R. Lopez, H. McWilliam, M. Remmert, J. Soding, J.D. Thompson, D.G. Higgins, Fast, scalable generation of high-quality protein multiple sequence alignments using Clustal Omega, Mol. Syst. Biol. 7 (2011) 539.
[53] R.J. Ganji, R. Reddi, R. Gumpena, A.K. Marapaka, T. Arya, P. Sankoju, S. Bhukya, A. Addlagatta, Structural basis for the inhibition of M1 family aminopeptidases by the natural product actinonin: Crystal structure in complex with E. coli aminopeptidase N, Protein Sci. 24 (5) (2015) 823–831.
[54] N. Drinkwater, N.B. Vinh, S.N. Mistry, R.S. Bamert, C. Ruggeri, J.P. Holleran, S. Loganathan, A. Paiardini, S.A. Charman, A.K. Powell, V.M. Avery, S. McGowan, P.J. Scammells, Potent dual inhibitors of Plasmodium falciparum M1 and M17 aminopeptidases through optimization of S1 pocket interactions, Eur. J. Med. Chem. 110 (2016) 43–64.
[55] Anthony Addlagatta, Xiaoyi Hu, Jun O. Liu, Brian W. Matthews, Structural basis for the functional differences between type I and type II human methionine aminopeptidases, Biochemistry 44 (45) (2005) 14741–14749.